Continuous Sound Velocity Measurements along the Shock Hugoniot Curve of Quartz

Mu Li,[1,2] Shuai Zhang,[2] Hongping Zhang,[1] Gongmu Zhang,[3] Feng Wang,[4] Jianheng Zhao,[1] Chengwei Sun,[1] and Raymond Jeanloz[2]

[1]*Institute of Fluid Physics, China Academy of Engineering Physics, Mianyang, Sichuan 621900, China*
[2]*Earth and Planetary Science, University of California, Berkeley, California 94720, USA*
[3]*Institute of Applied Physics and Computational Mathematics, Beijing 100094, China*
[4]*Laser Fusion Research Center, China Academy of Engineering Physics, Mianyang, Sichuan 621900, China*

(Received 25 December 2017; published 25 May 2018)

We report continuous measurements of the sound velocity along the principal Hugoniot curve of α quartz between 0.25 and 1.45 TPa, as determined from lateral release waves intersecting the shock front as a function of time in decaying-shock experiments. The measured sound velocities are lower than predicted by prior models, based on the properties of stishovite at densities below ~ 7 g/cm^3, but agree with density functional theory molecular dynamics calculations and an empirical wide-regime equation of state presented here. The Grüneisen parameter calculated from the sound velocity decreases from $\gamma \sim 1.3$ at 0.25 TPa to 0.66 at 1.45 TPa. In combination with evidence for increased (configurational) specific heat and decreased bulk modulus, the values of γ suggest a high thermal expansion coefficient at $\sim$0.25–0.65 TPa, where SiO_2 is thought to be a bonded liquid. From our measurements, dissociation of the molecular bonds persists to $\sim$0.65–1.0 TPa, consistent with estimates by other methods. At higher densities, the sound velocity is close to predictions from previous models, and the Grüneisen parameter approaches the ideal gas value.

DOI: 10.1103/PhysRevLett.120.215703

Shock and ramp compression offer reliable means of taking samples to ultrahigh pressures at which a variety of material properties can be measured [1,2]. In particular, sound velocity measurements characterize elasticity and cohesive energy as a function of density, both along the Hugoniot curve and for off-Hugoniot states [3]. The resulting equation of state is sensitive to the thermodynamic phase and electronic structure of the material [4]. Using lateral relaxation or overtaking by rarefaction waves [5], sound speed can be measured in steadily propagating shock-wave experiments. Moreover, unsteady wave techniques use a transparent standard material (e.g., α quartz SiO_2) [6,7], and our objective is to measure the sound velocity of this standard.

Silica is the most abundant oxide component of terrestrial mantles by weight and serves as a prototype for the dense silicates of planetary interiors [8,9]. While free SiO_2 is only expected in localized regions of Earth's mantle, the wider range of plausible compositions and higher $P-T$ conditions increase the possibilities for silica phases being present in exoplanets [8,10,11]. Hugoniot states from different initial states of SiO_2 have been extensively studied. In impendence-matching shock experiments, α quartz is used as a standard, but its Grüneisen coefficient is not well determined [12]. In the shocked liquid state, the nonlinear U_s-U_p relation [13,14] and excess configurational specific heat of silica need further characterization [15], as do the nonequilibrium states and time dependence of the material response [16,17].

A decaying shock samples a continuum of principal Hugoniot states, as the shock evolves over time and space [18,19]. Thermodynamic (electron-ion-phonon) equilibrium can be reached in $\sim$100 ps, or ~ 1 μm within the shock front, based on experimental observations [20] and calculations [21]. Although only possible for transparent materials, a decaying-shock experiment allows sound velocity to be measured continuously over a wide range of densities.

In this paper, we present continuous measurements of the sound velocity along the principal Hugoniot curve of α quartz up to TPa pressures, based on single-shot decaying shock experiments and using the bending of shock waves induced by lateral release waves. The bulk sound speed C_{bH} and Grüneisen coefficient $\gamma = V(dP/dE)_V$ are related as follows along the Hugoniot curve [1]:

$$C_{bH}^2 = -V^2\left(\frac{\partial P}{\partial V}\right)_S = \frac{1}{2}\gamma V P_H - V^2\left(\frac{dP}{dV}\right)_H\left[1-\frac{1}{2}\left(\frac{\gamma}{V}\right)(V_0-V)\right], \quad (1)$$

where P_H is pressure on the Hugoniot curve and $(dP/dV)_H$ is the slope of the Hugoniot curve at volume V, $(\partial P/\partial V)_S$ is the slope of the isentrope that intersects the Hugoniot curve at P_H, and subscript 0 indicates zero-pressure conditions. Using this approach, we can validate equation

of state (EOS) models for transparent materials over a wide range of densities.

The lateral-release method of determining sound velocity is rarely mentioned after the first attempts in the 1960s [5], because the precise location at which the shock front bends due to intersection with the rarefaction is difficult to determine. But line-imaging VISAR is now a standard instrument in shock experiments and allows us to detect a moving shock front in transparent samples. Also, the line-imaging VISAR has a spatial resolution as small as 5 μm, though this capacity is not often utilized. As the typical f value (focal distance-diameter) of lenses used is about 5, VISAR is sensitive to shock-front planarity. Lateral relaxation bends the shock front, and the reflected probe beam cannot go back into the VISAR system when the bending angle exceeds a threshold of ~2°–3°. This is illustrated in Fig. 1(a), where we see a sharp boundary between the bright planar shock front and the dim region of the bent shock front. This boundary corresponds to a near-constant bending angle, and its tangent allows us to deduce the sound speed as a function of shock velocity via

$$C_{bH}^2(t) = \{U_s(t)\tan[\alpha(t)]\}^2 + [U_s(t) - U_p(t)]^2, \quad (2)$$

where $U_s(t)$ is the shock velocity as a function of time t, and α is the angle between the shock direction and the tangent of the bending trace in X-Y space (perpendicular to and along the direction of shock propagation), as shown in Fig. 1(a). Also, $U_p(t)$ is the particle velocity behind the shock and can be obtained from the measured U_s-U_p relation.

Experiments were conducted using the 351 nm SG-III (prototype) laser system of the China Academy of Engineering Physics. Four beams with 2 mm diameter continuous phase plates yielded a total energy output of up to 3 kJ over 1 ns and generated a spatially uniform distribution of power density and hence sample loading. A ~5 μm CH film is deposited as an ablation layer to avoid significant preheat, and the pusher is a 40 μm layer of pure aluminum (Fig. 1). The stress pulse in the pusher can be tuned to be triangular in time, which is desirable for producing a decaying shock wave in the transparent sample. One edge of the sample is kept free, so as to generate lateral release waves.

When the shock wave breaks out of the pusher, it is incident onto the transparent sample and produces a propagating shock wave with lateral release from the bottom side of the sample as shown in Fig. 1(a). In X-Y space, the tangent of the bending boundary varies between 25° and 45° as a function of shock intensity, and the sample needs to be thick enough to let the streak camera distinguish the transverse displacement of the bending trace. In a transparent sample, the pressure behind the shock wave must be high enough to keep the moving shock front reflective, otherwise the VISAR signal is lost. In our experiments, the thickness of z-cut α quartz (2.65 g/cm^3, refractive index 1.547 at 532 nm wavelength) is 200 μm. On the surface adjacent to the aluminum pusher, a 200 nm thick aluminum layer was deposited on the sample to produce a reliable reflectivity that can be used as a reference. The processed vertical edge is placed as shown in Fig. 1(a), and this edge is perpendicular to both the plane of the figure and the slit of the streak camera, letting the

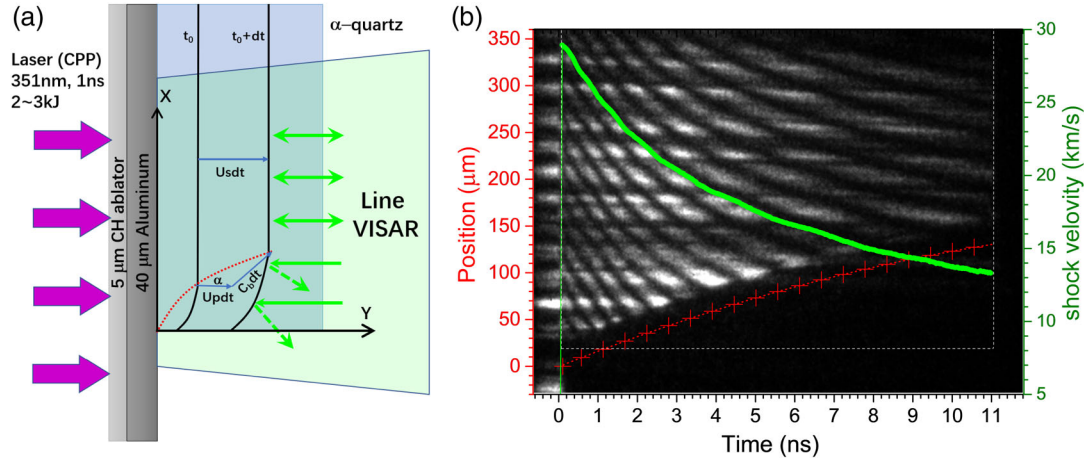

FIG. 1. (a) Experimental geometry: 4 beams of the SGIII (prototype) laser focused on the CH ablator produce an unsupported shock in the Al pusher. The quartz sample has a free side (shown at bottom of quartz sample) introducing a lateral release wave incident into the shock wave. The solid black curves indicate the shock front at different times, U_s is the shock wave velocity, U_p the particle velocity, and Cb the bulk sound velocity. The bent shock front below the red-dashed line scatters the reflected beam away from—rather than returning it to—the streak camera. (b) Line-imaging VISAR record for continuous sound-speed measurement from side release between shock incidence and breakout. The solid green curve shows the velocity of the shock front, and the red crosses (shifted downward by 20 μm) indicate the points at which the shock front bends and are used to extract the sound velocity along the Hugoniot curve.

camera record both the pusher (~150 μm) and the sample (~350 μm) in the X direction.

We measure the shock velocity and lateral release in the present experiments [Fig. 1(b)]. A line VISAR records two channels concurrently, the first using a 17-mm etalon for the velocity history. The second channel is used to enhance the image of the bending boundary, and we found that recording the reflected probe beam without the interferometer leg for this channel improves our results. The time variation for shock-wave entry into the quartz is less than 50 ps over ~500 μm diameter, so the shock front is planer and produces quasi-1D loading (see Supplemental Material [28] for details). To determine the absolute shock-velocity history, we take the transit thickness as a constraint ($\int U_S(t)dt =$ measured thickness of sample).

As can be seen in the streak-camera record, there is a boundary beyond which no signal returns from the shock front. Figure 1(b) shows the trace of the bending point and the shock velocity $U_s(t)$ over time, from which we get the position of the shock front, $Y(t)$. Then, from $Y(t)$ and $X(t)$, we get the bending points in X-Y space, and α is obtained as a function of shock velocity U_s and time t.

To calculate the sound speed according to Eq. (1), the pressure-volume relation of the principal Hugoniot curve must be known. Fortunately, high-precision data have been collected for quartz. For z-cut α quartz, $U_s = 6.278 + 1.193U_p - 2.505U_p \exp(-0.3701U_p)$ at pressures from 0.1 to 1.5 TPa (1 to 15 Mbar) [12], so we have pressure and volume along the Hugoniot curve as functions of the shock velocity. We then substitute the sound speed into Eq. (1), to obtain the Grüneisen parameter.

Figure 2 summarizes the sound velocity data, along with models from the present and prior work. The open squares [22] and stars [23] represent longitudinal sound velocity data for quartzite and crystal quartz, respectively, and the dash-dot-dot curve denotes sound velocity results of SiO_2 glass via Brillouin scattering in a diamond-anvil cell at room temperature [24]. Besides these direct measurements, Knudson and Desjarlais [12] used a Mie-Grüneisen equation of state to determine an analytic solution (hereafter called the "KD model") for the release isentrope as a function of shock velocity for quartz for $U_s > 15$ km/s, and their results are presented in Fig. 2. Sound velocity from density functional theory molecular dynamics (DFT-MD) calculations [25] and our newly developed wide regime equation of state (WEOS) empirical model [30] for silica are also shown (see Supplemental Material [25] for details).

The density of shocked α quartz in our experiments lies in the range 5.5 to 7.7 g/cm^3, and the corresponding pressure is from 0.25 to 1.45 TPa, which is far beyond the Hugoniot melting boundary [23,34]. The differences in sound velocity between shots 0401 and 0402 are mainly due to errors in the determination of the bending boundary of the moving shock front: the total transverse distance of the boundary is almost the thickness of sample, ~130 μm

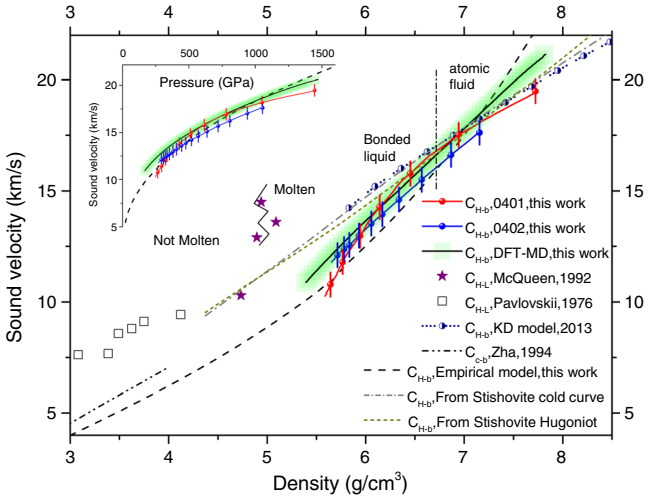

FIG. 2. Measured bulk sound velocity (red and blue filled circles with error bars) is in good agreement with DFT-MD calculations (solid black curve with green background), as well as our empirical EOS model (black dashed line). Subscript H means the Hugoniot state, b means bulk sound velocity, L means longitudinal sound velocity, and c means the cold state. Sound velocity from the analytic model (Knudson and Desjarlais [12], half-shaded circle) and previous data of Pavlovskii [22] (open squares), McQueen [23] (stars), and Zha [24] (dash-dot-dot curve) are indicated together with results from the cold curve [31,32] (dash-dotted curve) and the Hugoniot curve of stishovite [10,33] (short-dashed curve).

here, but the spatial resolution of VISAR is about 5 μm. Although the maximum discrepancy of sound speed is ~1 km/s, the trend and average of results from the 2 experiments agree with each other. The measured bulk sound velocity (blue and red curves in Fig. 2) agree with our WEOS model and DFT-MD calculations for densities below ~7 g/cm^3. All of our results for the sound velocity are slightly lower than those from the KD model in this range [12], with the value at 250 GPa being much lower than has been measured at the melting boundary [23]. Our results approach the KD model at higher densities, merging at ~6.5–7 g/cm^3 (~650–950 GPa, ~30 000–47 000 K).

Based on the sound velocity data in Fig. 2, the Grüneisen parameter along the quartz Hugoniot curve can be calculated via Eq. (1), and is shown in Fig. 3. The experimental Grüneisen parameters decrease monotonically as density increases, and approach 0.66 (value for the ideal gas) at densities of ~7–7.5 g/cm^3.

Average Grüneisen parameter values obtained from the differences between distinct thermodynamic paths $[\bar{\gamma} \approx V(\Delta p/\Delta E)_V]$ are shown in Fig. 3 for reference, because these curves can help distinguish temperature and volume dependencies of gamma. The blue dash-dot curve is the average between the Hugoniot curves of fused silica [14] and quartz [12], and the green dash curve is the average between the Hugoniot curve of quartz [12] and the cold curve of stishovite [31,32]. The density of quartz is

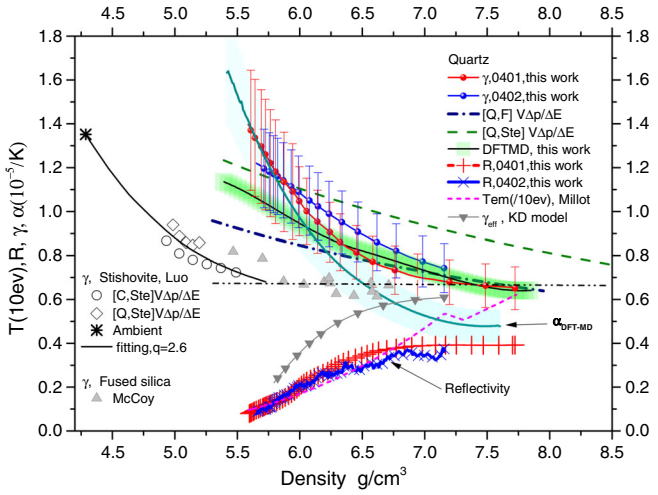

FIG. 3. Calculated Grüneisen parameter of SiO_2 decreases with compression, and approaches 0.66 at densities above 7.0 g/cm^3. The solid closed circles (red and blue) give the present measurements, the dark blue dash-dot curve is the average value ($\bar{\gamma}_{FQ}$) between the Hugoniot curves of fused silica [14] and quartz [12], and the olive dashed curve is the average value ($\bar{\gamma}_{QS}$) between the quartz Hugoniot curve [12] and the stishovite cold curve [31,32]. The black solid curve with green shading shows the DFT-MD result. Inverted triangles show the effective gamma in the KD model [12]. The black solid and open symbols on the left side are data for solid stishovite [35], and gray triangles are data for liquid fused silica [7]. The solid cyan gives the calculated thermal expansion coefficient (α). Reflectivity (R) measured from the shock front using the VISAR probe laser (blue × s and red bars) and the Hugoniot temperature (T, purple short dash) calibrated by Millot *et al.* [10] are also shown.

between those of fused silica and stishovite, so its Hugoniot temperature is also intermediate. It is clear that our experimental data and DFT-MD results lie between $\bar{\gamma}_{FQ}$ and $\bar{\gamma}_{QS}$, and the Grüneisen parameter decreases with temperature over the experimental pressure range. The low-density data for fused silica [7] shown in Fig. 3 lie below $\bar{\gamma}_{FQ}$, and all the higher-density data are for the liquid state. Luo [35] presents data for solid stishovite in the lower-density range. We find that the average gamma $\bar{\gamma}_{QS}$ jumps from 0.85 to 1.23 upon shock melting, with our data above 1.23 at the lower end of our experimental range.

For molten silica, we also distinguish between bonded liquid and atomic liquid after Hicks *et al.* [15]. Hicks *et al.* [15] used excess configurational specific heat (average value minus model ignoring chemical bonds) as evidence for a bonded liquid. Knudson's calculations [13] indicate that the extended region of curvature in the U_s-U_p Hugoniot curve is due to disorder and dissociation of the fluid, but the curvature of U_s-U_p is hard to determine precisely via classical shock Hugoniot experiments. In the present experiment, we find that bulk sound velocity can offer constraints on the presence of chemical bonds based on a thermodynamically consistent analysis of sound velocity. Stixrude *et al.* [31,32] and Nissim *et al.* [36] developed an analytical method to calculate the sound velocity of solid matter throughout $P-\rho$ phase-space, by using the Grüneisen equation of state and knowledge of the cold curve. This model is valid for metals [36,37] even to very high pressures, regardless of the effects of chemical bonds and, hence, may also be valid for atomic fluid silica.

We calculate the bulk sound velocity along the Hugoniot curve of α quartz based on the finite strain EOS for the cold curve and Hugoniot curve of stishovite [38]. A self-consistent relation for the isothermal bulk modulus is [31,32],

$$\begin{aligned} K_s &= \rho C_b^2 = K_T + \gamma^2 \rho C_V T \\ &= (1+2f)^{5/2}\left[K_{0T} + (3K_{0T}K'_{0T} - 5K_{0T})f \right. \\ &\quad \left. + \frac{27}{2}(K_{0T}K'_{0T} - 4K_{0T})f^2\right] \\ &\quad + (\gamma + 1 - q)\gamma\rho\Delta E_q - \gamma^2\rho\Delta(C_V T) + \gamma^2\rho C_V T \\ &= K_{cs} + (\gamma + 1 - q)\gamma\rho\Delta E_q, \end{aligned} \tag{3}$$

where $f = \frac{1}{2}[(\rho/\rho_{0s})^{2/3} - 1]$ is the Eulerian strain, K_s is the isentropic bulk modulus, C_b is bulk sound velocity, K_{0T}(334 GPa) is the initial isothermal bulk modulus of stishovite, C_V is the constant-volume heat capacity, K'_{0T} (4.0) is the pressure derivtive $(dK_T/dP)_0$, ρ_{0s} (4.287 g/cm^3) is the initial density of stishovite, K_{cs} is the isentropic bulk modulus for the cold reference state, ΔE_q is the change in thermal energy from the reference state, q is $\partial \ln\gamma/\partial \ln V$ and close to unity ($q \approx 1$), $\gamma_0 = 1.35$, and the energy of transition from quartz to stishovite is $E_{\mathrm{Tr}} = 0.89$ MJ/kg [39]. Note that K_S is insensitive to the value of γ, and we chose parameters for the $CaCl_2$-type SiO_2 rather than the octahedrally coordinated stishovite because the pressure here is much higher than the transition of quartz to stishovite [32]. For calculations from the stishovite Hugoniot data [10,33], the reference state changes from the cold curve to the Hugoniot curve.

The calculated quartz Hugoniot sound velocity based on stishovite is shown in Fig. 2. The gray dash-dot curve is from the cold-compression curve, and the olive short dash curve is from the Hugoniot curve. The two sets of results are consistent with each other, and comparable with the KD model results throughout the density range shown in Fig. 2. Our experimental measurements, DFT-MD calculations, and WEOS model are also comparable with these results at higher densities, but below them at densities of 5.5–6.5 g/cm^3. Along the Hugoniot curve, the KD model is consistent with Eq. (1) and only relies on γ_{eff}, which is reasonable at high densities (>7 g/cm^3 in Fig. 3). The agreement at densities higher than ~7 g/cm^3 suggests that the sound velocity is close to the results of Eq. (3) for the atomic fluid, and the discrepancy at lower densities is from the effects of chemical bonding that are not reflected in Eq. (3).

Our experimental sound velocity measurements merge with the results of Eq. (3) at densities of ~6.5–7 g/cm^3

(~0.65–1.0 TPa, ~30 000–50 000 K). The experimentally estimated temperature [10] shows a nearly linear increase with shock velocity, and the optical reflectivity stops changing at densities of ~7–7.5 g/cm^3. The temperature jump at $U_s = 24 \sim 25$ km/s may be due to absorption from the unshocked sample, and new detailed DFT-MD calculations show a continuous slope from low pressure up to 2 TPa [40]. The sound velocity, reflectivity, and temperature observations are consistent with each other in indicating the end of silica dissociation at densities above 7 g/cm^3, compatible with previous estimates (from 550 GPa [41], 650 GPa [15], to 1.2 TPa [13]) but requiring further refinement and verification.

The Grüneisen parameter γ and thermal expansion coefficient α are closely linked, with Eq. (3) and the definition of α giving $\alpha = C_V\gamma\rho/K_T = \gamma/[(C_b^2/C_V) - \gamma^2 T]$. At these pressure-temperature conditions in bonded liquid silica, the heat capacity is higher than the Dulong-Petit limit [15], the sound velocity is lower, and γ is higher than the KD model estimates, implying higher values for the thermal expansion coefficient in the bonded liquid phase, as supported by our DFT-MD calculations (Fig. 3). The value of α of liquid silica at 300 GPa shock pressure is closer to that of solid α quartz (~10^{-5}/K) than of liquid silica (near zero) at ambient pressure.

To summarize, we measured the bulk sound velocity along the principal Hugoniot curve of z cut α quartz using lateral release of decaying single-shot states from 0.25 to 1.45 TPa. This is the first direct measurement of sound velocity at such high pressures, and the results are in good agreement with DFT-MD calculations. The bulk modulus of bonded liquid silica shocked from α quartz is lower than previously estimated, which may be due to high specific heat and high thermal expansion coefficient. From our measurements, dissociation of the molecular bonds persists to ~0.65–1.0 TPa, consistent with estimates by other methods. Continuous measurement of sound velocity along the Hugoniot curve is demonstrated to constrain the equation of state and Grüneisen parameter of transparent samples to very high pressures, which is of great interest for mineral physics and planetary science as well as other areas of high energy-density physics.

We thank the crew of the Laser Fusion Research Center SGIII (Proto) facility for their contributions to these experiments. This research is sponsored by National Natural Science Foundation of China, Contracts No. 11172280 and No. 11472255.

[1] J. W. Forbes, Shock wave compression of condensed matter, a primer, in *Shock Wave and High Pressure Phenomena*, edited by R. A. Graham, L. Davison, and Y. Horie (Springer, Berlin Heidelberg, 2012).

[2] R. F. Smith *et al.*, Ramp compression of diamond to five terapascals, Nature (London) **511**, 330 (2014).

[3] W. A. Harrison, *Electronic Structure and the Properties of Solids* (Dover, New York, 1989).

[4] R. Jeanloz, Shock wave equation of state and finite strain theory, J. Geophys. Res. Solid Earth **94**, 5873 (1989).

[5] L. V. Al'tshuler *et al.*, The isentropic compressibility of aluminium, copper, lead and iron at high pressures, Sov. Phys. JETP **11**, 766 (1960).

[6] D. E. Fratanduono, D. H. Munro, P. M. Celliers, and G. W. Collins, Hugoniot experiments with unsteady waves, J. Appl. Phys. **116**, 033517 (2014).

[7] C. A. McCoy, M. C. Gregor, D. N. Polsin, D. E. Fratanduono, P. M. Celliers, T. R. Boehly, and D. D. Meyerhofer, Measurements of the sound velocity of shock-compressed liquid silica to 1100 GPa, J. Appl. Phys. **120**, 235901 (2016).

[8] T. Duffy, N. Madhusudhan, and K. K. M. Lee, 2.07—Mineralogy of super-earth planets, in *Treatise on Geophysics*, 2nd ed., edited by G. Schubert (Elsevier, Oxford, 2015), p. 149.

[9] S.-N. Luo, J. A. Akins, T. J. Ahrens, and P. D. Asimow, Shock-compressed $MgSiO_3$ glass, enstatite, olivine, and quartz: Optical emission, temperatures, and melting, J. Geophys. Res. **109**, (B5) (2004).

[10] M. Millot, N. Dubrovinskaia, A. Černok, S. Blaha, L. Dubrovinsky, D. G. Braun, P. M. Celliers, G. W. Collins, J. H. Eggert, and R. Jeanloz, Shock compression of stishovite and melting of silica at planetary interior conditions, Science **347**, 418 (2015).

[11] D. K. Spaulding, R. S. McWilliams, R. Jeanloz, J. H. Eggert, P. M. Celliers, D. G. Hicks, G. W. Collins, and R. F. Smith, Evidence for a Phase Transition in Silicate Melt at Extreme Pressure and Temperature Conditions, Phys. Rev. Lett. **108**, 065701 (2012).

[12] M. D. Knudson and M. P. Desjarlais, Adiabatic release measurements in α-quartz between 300 and 1200 GPa: Characterization of α-quartz as a shock standard in the multimegabar regime, Phys. Rev. B **88**, 184107 (2013).

[13] M. D. Knudson and M. P. Desjarlais, Shock Compression of Quartz to 1.6 TPa: Redefining a Pressure Standard, Phys. Rev. Lett. **103**, 225501 (2009).

[14] C. A. McCoy, M. C. Gregor, D. N. Polsin, D. E. Fratanduono, P. M. Celliers, T. R. Boehly, and D. D. Meyerhofer, Shock-wave equation-of-state measurements in fused silica up to 1600 GPa, J. Appl. Phys. **119**, 215901 (2016).

[15] D. G. Hicks, T. R. Boehly, J. H. Eggert, J. E. Miller, P. M. Celliers, and G. W. Collins, Dissociation of Liquid Silica at High Pressures and Temperatures, Phys. Rev. Lett. **97**, 025502 (2006).

[16] A. E. Gleason *et al.*, Ultrafast visualization of crystallization and grain growth in shock-compressed SiO_2, Nat. Commun. **6**, 8191 (2015).

[17] A. Denoeud, S. Mazevet, F. Guyot, F. Dorchies, J. Gaudin, A. Ravasio, E. Brambrink, and A. Benuzzi-Mounaix, High-pressure structural changes in liquid silica, Phys. Rev. E **94**, 031201 (2016).

[18] J. H. Eggert, D. G. Hicks, P. M. Celliers, D. K. Bradley, R. S. McWilliams, R. Jeanloz, J. E. Miller, T. R. Boehly, and G. W. Collins, Melting temperature of diamond at ultrahigh pressure, Nat. Phys. **6**, 40 (2010).

[19] P. M. Celliers, D. K. Bradley, G. W. Collins, D. G. Hicks, T. R. Boehly, and W. J. Armstrong, Line-imaging velocimeter for shock diagnostics at the OMEGA laser facility, Rev. Sci. Instrum. **75**, 4916 (2004).

[20] T. Löwer, V. N. Kondrashov, M. Basko, A. Kendl, J. Meyer-ter-Vehn, R. Sigel, and A. Ng, Reflectivity and Optical Brightness of Laser-Induced Shocks in Silicon, Phys. Rev. Lett. **80**, 4000 (1998).

[21] A. Ng and T. Ao, Nonequilibrium and Non-Steady-State Evolution of a Shock State, Phys. Rev. Lett. **91**, 035002 (2003).

[22] M. N. Pavlovskii, Measurements of the velocity of sound in shock-compressed quartzite, dolomite, anhydrite, sodium chloride, paraffin, plexiglas, polyethylene, and fluoroplast-4, J. Appl. Mech. Tech. Phys. **17**, 709 (1976).

[23] R. G. McQueen, The Velocity of Sound behind Strong Shocks in SiO_2, in *Shock Compression of Condensed Matter–1991*, edited by R. D. Dick, J. W. Forbes, and D. G. Tasker (Elsevier, Amsterdam 1992), p. 75.

[24] C.-s. Zha, R. J. Hemley, H. K. Mao, T. S. Duffy, and C. Meade, Acoustic velocities and refractive index of SiO_2 glass to 57.5 GPa by Brillouin scattering, Phys. Rev. B **50**, 13105 (1994).

[25] See Supplemental Material at http://link.aps.org/supplemental/10.1103/PhysRevLett.120.215703 for more experimental information, detailed description of the WEOS model and the DFT-MD calculations, which includes Refs. [26–29].

[26] D. M. Ceperley and B. J. Alder, Ground State of the Electron Gas by a Stochastic Method, Phys. Rev. Lett. **45**, 566 (1980).

[27] J. P. Perdew and A. Zunger, Self-interaction correction to density-functional approximations for many-electron systems, Phys. Rev. B **23**, 5048 (1981).

[28] P. E. Blöchl, Projector augmented-wave method, Phys. Rev. B **50**, 17953 (1994).

[29] G. Kresse and J. Furthmüller, Efficient iterative schemes for *ab initio* total-energy calculations using a plane-wave basis set, Phys. Rev. B **54**, 11169 (1996).

[30] H. Liu *et al.*, Validation for equation of state in wide regime: Copper as prototype, Matter Radiat. Extremes **1**, 123 (2016).

[31] L. Stixrude and C. Lithgow-Bertelloni, Thermodynamics of mantle minerals—I. Physical properties, Geophys. J. Int. **162**, 610 (2005).

[32] D. Andrault, R. J. Angel, J. L. Mosenfelder, and T. Le Bihan, Equation of state of stishovite to lower mantle pressures, Am. Mineral. **88**, 301 (2003).

[33] S.-N. Luo *et al.*, Direct shock wave loading of Stishovite to 235 GPa: Implications for perovskite stability relative to an oxide assemblage at lower mantle conditions, Geophys. Res. Lett. **29**, 36 (2002).

[34] J. A. Akins and T. J. Ahrens, Dynamic compression of SiO_2: A new interpretation, Geophys. Res. Lett. **29**, 31 (2002).

[35] S.-N. Luo, J. L. Mosenfelder, P. D. Asimow, and T. J. Ahrens, Stishovite and its implications in geophysics: New results from shock-wave experiments and theoretical modeling, Phys. Usp. **45**, 435 (2002).

[36] N. Nissim, S. Eliezer, and M. Werdiger, The sound velocity throughout the P-ρ phase-space with application to laser induced shock wave in matter precompressed by a diamond anvil cell, J. Appl. Phys. **115**, 213503 (2014).

[37] X. Gao, L. Chen, R. Valencia, W. Xia, W. Gao, X.-Y. Han, J.-M. Li, and P. Zhang, *Ab initio* study of thermodynamically consistent equation of state of warm dense aluminum plasma, Phys. Plasmas **23**, 092710 (2016).

[38] D. Andrault *et al.*, Pressure-induced Landau-type transition in stishovite, Science **282**, 720 (1998).

[39] W. R. Panero, L. R. Benedetti, and R. Jeanloz, Equation of state of stishovite and interpretation of SiO_2 shock-compression data, J. Geophys. Res. **108**, ECV 5-1 (2003).

[40] T. Qi, M. Millot, R. G. Kraus, S. Root, and S. Hamel, Optical and transport properties of dense liquid silica, Phys. Plasmas **22**, 062706 (2015).

[41] G. I. Kerley, *Equations of State for Composite Materials* (Sandia National Laboratories, Albuquerque, NM, 1999).